Frequency-Resolved Nonlinear Turbulent Energy Transfer into Zonal Flows in Strongly Heated *L*-Mode Plasmas in the HL-2A Tokamak

M. Xu,[1,2] G. R. Tynan,[1,2] P. H. Diamond,[1,3,4] P. Manz,[1,2] C. Holland,[2] N. Fedorczak,[1,2] S. Chakraborty Thakur,[1,2] J. H. Yu,[2] K. J. Zhao,[5] J. Q. Dong,[5,6] J. Cheng,[5] W. Y. Hong,[5] L. W. Yan,[5] Q. W. Yang,[5] X. M. Song,[5] Y. Huang,[5] L. Z. Cai,[5] W. L. Zhong,[5] Z. B. Shi,[5] X. T. Ding,[5] X. R. Duan,[5] Y. Liu,[5] and HL-2A team

[1]*Center for Momentum Transport and Flow Organization, University of California at San Diego, California 92093, USA*
[2]*Center for Energy Research & Department of Mechanical and Aerospace Engineering, University of California at San Diego, California 92093, USA*
[3]*Center for Astrophysics and Space Science & Department of Physics, University of California at San Diego, California 92093, USA*
[4]*WCI Center for Fusion Theory, NFRI, Gwahangno 113, Yusung-gu, Daejeon 305-333, Korea*
[5]*Southwestern Institute of Physics, P.O. Box 432, Chengdu 610041, China*
[6]*Institute for Fusion Theory and Simulation, Zhejiang University, Hangzhou 310058, China*

(Received 2 November 2011; published 11 June 2012)

The absolute rate of nonlinear energy transfer among broadband turbulence, low-frequency zonal flows (ZFs) and geodesic acoustic modes (GAMs) was measured for the first time in fusion-grade plasmas using two independent methods across a range of heating powers. The results show that turbulent kinetic energy from intermediate frequencies (20–80 kHz) was transferred into ZFs and GAMs, as well as into fluctuations at higher frequencies ($>$ 80 kHz). As the heating power was increased, the energy transfer from turbulence into GAMs and the GAM amplitudes increased, peaked and then decreased, while the energy transfer into the ZFs and the ZFs themselves increased monotonically with heating power. Thus there exists a competition between ZFs and GAMs for the transfer of turbulent energy, and the transfer into ZFs becomes dominant as the heating power is increased. The poloidal-radial Reynolds stress and the mean radial electric field profiles were also measured at different heating powers and found to be consistent with the energy transfer measurement. The results suggest that ZFs play an important role in the low-to-high (*L*-*H*) plasma confinement transition.

DOI: 10.1103/PhysRevLett.108.245001 PACS numbers: 52.25.Fi, 52.35.Mw, 52.35.Ra

Zonal flows are widely observed in nature, such as the Jovian belts and zones, the terrestrial atmospheric jet stream, in the differential rotation of the sun, and in the laboratory in low temperature linear plasma devices, rotating neutral fluids and tokamak fusion devices. They coexist with and are nonlinearly excited by small-scaled turbulent fluctuations [1–3] and are thought to play a key role in determining the rate of turbulent mixing in confined plasmas and other systems. The question of how large-scale zonal flows self-organize from a background of small-scale fluctuations is thus a fundamental issue in both magnetic fusion and astrophysics research. Moreover, because zonal flows are a general phenomenon, a deeper understanding of the zonal flow-turbulence system, and of the competition and spatial structure selection process occurring between low-frequency zonal flows (ZFs) and geodesic acoustic modes (GAMs), naturally leads to a deeper understanding of self-organization processes in many systems of scientific interest.

In fusion plasmas the importance of spontaneously generated large-scale sheared flows such as ZFs and GAMs has long been recognized since they can regulate the turbulent transport via a multiscale fluctuations interaction process [4,5]. Substantial experimental evidences have led to a general acceptance of the roles that ZFs and GAMs play in regulating core plasma transport [1,6–8]. Furthermore, recent work in several tokamak devices [9–14] suggests that time-varying sheared zonal flows may play an important role in the low-to-high (*L*-*H*) confinement transition. As a result, the physics of turbulence-ZF interactions in strongly heated *L*-mode plasmas which are approaching the *H*-mode transition threshold is of particular importance.

In this Letter, we report the first systematic experimental study of the turbulent Reynolds stress and nonlinear energy transfer rate at the plasma boundary as the heating power approaches the *L*-*H* transition threshold. In particular, we provide the first experimentally measured frequency-resolved energy transfer rates between turbulence and zonal flows in fusion plasmas using a newly developed multifield cross-bispectral method [15]. Although bispectral analysis has been used to evaluate the nonlinear coupling strength before [16,17], the previously reported quantities are *normalized* bispectra, i.e., the bicoherence, which can only tell that turbulence and zonal flows are phase-correlated [18,19], leaving the critical questions of energy transfer rate and direction unanswered. In addition, in earlier work on tokamak devices the energy transfer was measured using a single field turbulence model [20], which is problematic in the edge of tokamak plasmas since the density and potential are significantly decorrelated and thus exhibit different dynamics. In those cases where multifield approaches

were used the work was conducted on small laboratory plasmas [21–26]. Previous time-domain estimates of the turbulence production term [18,19,26] in confinement experiments gives the energy transfer rate in real units, but this approach does not allow a determination of which frequencies lose energy and which frequencies receive energy. Here we compute the energy transfer rates using both frequency-resolved bispectra and time-domain methods, and find the results to be consistent. Furthermore we then use these approaches to make the first systematic study of the evolution of the nonlinear coupling of turbulence to ZFs and GAMs as the L-H transition is approached. The results show that turbulent fluctuations drive both ZFs and GAMs through nonlinear interactions; i.e., these large-scale shear flows are amplified by the transfer of kinetic energy and momentum out of the ambient drift wave spectrum [1,27,28]. The ZFs and GAMs compete with each other for the transfer of turbulent energy, and the transfer of turbulent energy into ZFs begins to dominate as the plasma auxiliary heating begins to dominate the total heat input to the plasma. This observed branching phenomenon is consistent with a newly proposed shear mode competition model [29]. If these trends continue to the L-H power threshold, the results suggest that ZFs would play an important role in the L-H plasma confinement transition.

The experiments were carried on the HL-2A tokamak [30–32] which has a major radius of 1.65 m and a minor radius of 0.4 m. It is equipped with 2 MW electron cyclotron resonance heating (ECRH) at 68 GHz, 1 MW lower hybrid current drive (LHCD) at 2.45 GHz, and 1.5 MW neutral beam injection (NBI). For these experiments up to ~700 kW of ECRH power was used. At the typical discharge conditions for this experiment ($B = 1.35$ T, ECRH up to 730 kW, $Ip \sim 150$ kA with a loop voltage of about 1 Volt, giving an Ohmic heating of 150 kW) the chord averaged density measured by an HCN laser interferometer is about $1–2 \times 10^{19}/\mathrm{m}^3$, and the edge plasma safety factor is about 4.3. To make the required edge plasma measurements, a multi-tipped probe array was inserted into the plasma to measure time-averaged profiles and fluctuations. The Langmuir probe array is composed of two symmetric 3×4 probe arrays (21 tips total), with one 3×4 array (3 tips along the poloidal direction and 4 in the radial direction) facing in the same direction as the plasma current, I_p, while the other faces the counter Ip direction. With this symmetry a comparison between these two arrays facing the co- and countercurrent directions can be done to estimate shadowing effects on the fluctuation measurements. With a proper setup, this probe array can simultaneously measure plasma density, potential, temperature, Reynolds stress, particle flux, and vorticity flux, etc. The distance between two adjacent probe tips is 5 mm in the poloidal direction and 2.5 mm in the radial direction, which makes the 3×4 array smaller than a typical turbulent eddy in both poloidal and radial directions (in HL-2A tokamak edge plasma the typical turbulent correlation length in the poloidal direction is bigger than 3 cm and in the radial direction is ~1.0–1.5 cm [32]).

Figures 1(a) and 1(b) show equilibrium profiles of plasma density and electron temperature. As the heating increases from purely Ohmic heating to Ohmic + ECRH heating, the plasma density profile is unchanged [Fig. 1(a)] while the electron temperature [Fig. 1(b)] increases by 30%–80% from Ohmic (black diamonds) to 730 kW ECRH heating (red squares) within the last close flux surface (LCFS). The plasma space potential was estimated using $\phi_{\mathrm{plasma}} \approx \phi_{\mathrm{float}} + \frac{1}{2}\ln\left(\frac{m_i}{2\pi m_e}\frac{T_e}{ZT_e+T_i}\right) \approx \phi_{\mathrm{float}} + 2.8T_e$, where ϕ_{plasma} is the plasma potential, ϕ_{float} is the floating potential, m_i/m_e is the ion-electron mass ratio, T_e and T_i are the electron and ion temperature, respectively, Z is the ion charge state [33]. The radial electric field, shown in Fig. 1(c), was inferred from the gradient of the plasma space potential using a time average with 2 ms time window. Figure 1(d) shows the plasma fluctuation velocity in the poloidal direction, which was inferred using time-delay estimation (TDE) from poloidally separated tips [34]. It shows that the fluctuations propagate in the electron diamagnetic direction inside the LCFS and in the ion diamagnetic direction outside the LCFS, consistent with similar observations in many other confinement experiments. Here the flow reversal position was used as a reference to identify the LCFS position. The flow velocity estimated by TDE is about 30% larger than the mean $E \times B$ velocity obtained from mean Er shown in Fig. 1(c), and is thought to be a combination of fluid $E \times B$ and the turbulence phase velocity, again consistent with earlier results. The difference in the combined poloidal velocities for different heating powers, shown in Fig. 1(d), is not as pronounced as in Fig. 1(c).

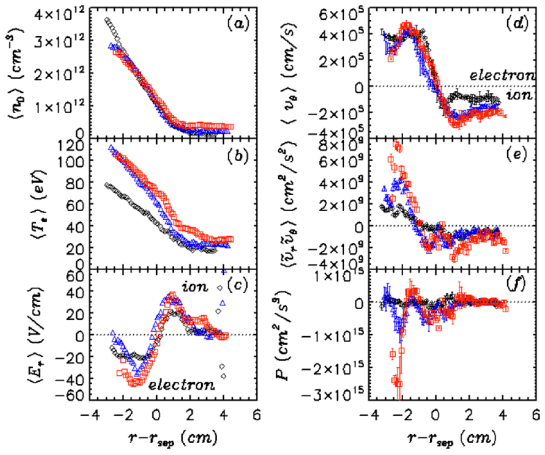

FIG. 1 (color online). Profiles at different ECRH heating power. Black diamond is pure Ohmic plasma, blue triangle is for 380 kW ECRH, and red square is for 730 kW ECRH. The x axis is the radial position corresponding to r-r_{sep}. (a) Time-averaged density measured by the probe array. (b) Electron temperature. (c) Estimated mean electric field. (d) Poloidal velocity calculated using two-point time-delay estimation. (e) Turbulent Reynolds stress, and (f) the inferred energy transfer.

Figures 2(a) and 2(b) show the autospectra of potential and perpendicular velocity fluctuations $\propto (\nabla_\perp \phi)^2$ respectively at different ECRH powers at a position ~2.5 cm inside the LCFS. Both figures show clearly separated low frequency ZFs (for frequency $f < 1$–2 kHz), GAMs (centered at $f \sim 10$ kHz), and turbulence regions with $f >$ 15 kHz, consistent with earlier results from this device [30–32,35,36]. A pronounced feature is that the power associated with ZFs increased by a factor of more than 100 when the ECRH power was increased from 0 to 730 kW. This is a clear indication that much stronger ZFs developed as the plasma heating was increased. As shown in Fig. 1(e), there is a large negative gradient of Reynolds stress that exists in between −2 cm to LCFS, which shows that there is a concentration of positive turbulent angular momentum within this region due to turbulent transport [4]. Here "positive" corresponds to the electron diamagnetic direction. The position of this negative gradient coincides with a large positive poloidal $E \times B$ flow and fluctuation propagation as is shown in Fig. 1(c) and 1(d), consistent with the accumulation of positive turbulent momentum in this region. Also note that the gradient of Reynolds stress within the region from r-$r_{\rm sep} = -2$ cm out to the LCFS increased by a factor of 4–5 as the ECRH heating increased from 0 to 730 kW [indicated by the black diamonds and red squares in Fig. 1(e)]. Since the Reynolds force is expressed as $F_{\rm pol} = m_{\rm plasma} \frac{\partial \langle v_\theta \rangle}{\partial t} = -m_{\rm plasma} \frac{\partial}{\partial r} \langle \tilde{v}_r \tilde{v}_\theta \rangle$ [4], the Reynolds force exerted on the mean flow was also increased and therefore should lead to a larger mean $E \times B$ velocity consistent with the estimated mean $E \times B$ flow in Fig. 1(c). The negative radial electric field inside the LCFS [− 2 to 0 cm in Fig. 1(c)] was more than doubled as the power was increased, indicating that a stronger mean $E \times B$ flow was developed as the heating power ramped up. The decorrelation rate due to mean shear can be estimated as $|\omega_{\rm shear}| \approx |\frac{\partial \langle v_\theta \rangle}{\partial r}| \sim 3 \times 10^5$ Hz for $P_{\rm ECH} = 730$ kW using the poloidal $E \times B$ velocity estimated from electric field profile shown in Fig. 1(c), and the eddy rotation rate can also be estimated as $\omega_{\rm eddy} \approx \tau_{\rm eddy}^{-1} \approx \frac{|\tilde{\phi}_f|}{BL_r L_{\rm pol}} \approx 0.4$–$1.2 \times 10^5$ Hz [24]. Here B is the toroidal field ~1.35 Tesla, and $|\tilde{\phi}_f|$ is the floating potential fluctuation amplitude and is typically $|\tilde{\phi}_f| \sim 30$–50 V for a 730 kW discharge. The turbulent eddy sizes in the radial direction $L_r \sim 1$ cm and in the poloidal direction $L_{\rm pol} \sim 3$–5 cm were used [32]. Therefore we find that the turbulent stress is acting to reinforce the shear flow inside the LCFS, this effect becomes more pronounced at higher heating powers, and for the highest heating power used here, we have $|\omega_{\rm shear}| > \omega_{\rm eddy}$, showing that at least at 730 kW of ECRH heating the mean shear becomes strong enough to affect the turbulence dynamics via the usual shear decorrelation mechanism.

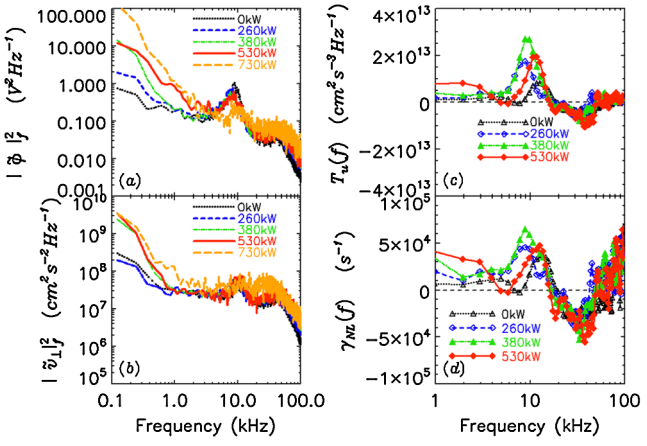

FIG. 2 (color online). At different ECRH power (a) frequency spectrum of potential fluctuations and (b) of perpendicular velocity fluctuations. (c) Nonlinear kinetic energy transfer rate. (d) Effective growth rate due to nonlinear energy transfer.

The mean velocity and Reynolds stress profiles were used to estimate the energy transfer between mean flow and turbulence in the time domain [18,19,26] to compare with the frequency-domain measurements presented below. The energy transfer between mean flow and fluctuations could be estimated as $P = -\langle \tilde{v}_r \tilde{v}_\theta \rangle \frac{\partial \langle v_\theta \rangle}{\partial r}$. Here the averaging time window is determined from previous frequency-resolved measurements which have isolated the ZFs, GAMs and turbulent fluctuations [32]. Since in normal fluids with 3-D dynamics, P corresponds to a turbulent Reynolds stress working against mean flow to generate fluctuations, it is also called the turbulence production rate. When P is negative, it means that net energy is transferred from the turbulence into mean flow. When calculating the time average $\langle \ldots \rangle$, a two-millisecond window was used and turbulent fluctuations are computed by applying a high pass (> 20 kHz) digital filter to measured data. As the time average serves as a low-pass filter, here mean flow actually refers to the flows with fluctuation frequencies below a few hundred Hz and the energy transfer rate inferred is actually the energy exchange between turbulence (with $f > 20$ kHz) and such mean flows. Figure 1(f), shows the turbulent production term, P, inferred from the Reynolds stress and mean sheared velocity profiles. The results show that for all heating powers in the region between −2 cm to 2 cm we find that $P < 0$, meaning that in this region net energy is transferred from turbulent fluctuations into low-frequency flows. Furthermore, at $r - r_{\rm sep} \sim -2$ cm, as the heating power was increased, the production term P increased from almost zero for Ohmic plasma to -1×10^{15} cm^2/s^3 for 380 kW, and then to -3×10^{15} cm^2/s^3 for 730 kW heating power, as indicated in Fig. 1(f) by the black, blue, and red colors.

To gain a clearer understanding of this behavior, we next examine the associated nonlinear energy transfer in the frequency domain. The 2D frequency-resolved nonlinear energy transfer [23] for Ohmic and 530 kW ECRH discharges are shown in Figs. 3(a) and 3(b) respectively, which were computed from more than 300 ensembles of time-stationary data taken roughly at r-$r_{\rm sep} = -2.5$ cm. A positive value (red or yellow) at (f, $f1$) means that the

frequency f associated with perpendicular velocity fluctuation (x axis) gains energy and a negative value (blue) means that perpendicular velocity fluctuation at frequency f loses energy. With the help of the 2D f-$f1$ energy transfer in Figs. 3(a) and 3(b), we conclude that the ZFs' and GAMs' nonlinear energy gain mostly comes from the interactions with turbulent frequencies ranging between 20–80 kHz and the energy transfer rate into the shear flows increases substantially as the heating power is increased.

The net frequency-resolved nonlinear energy transfer, shown in Fig. 2(c), can be obtained by integrating the 2D f-$f1$ energy transfer over $f1$. Alternatively, recognizing that this can also be recast as a cross-spectrum $T_v(f) = -\mathrm{Re}\sum_{f_1}\langle \vec{v}^*_{\perp f} \cdot (\vec{v}_{\perp f-f_1} \cdot \nabla_\perp \vec{v}_{\perp f_1})\rangle = -\mathrm{Re}\langle F(\vec{v}_\perp)^* \cdot F(\vec{v}_\perp \cdot \nabla_\perp \vec{v}_\perp)\rangle$, where "$F$" indicates the Fourier transform and "*" means the complex conjugate, we can also compute the net frequency-resolved energy transfer from a synthesized time-series computed from measured data. The results [see Fig. 2(c)] and the corresponding 2D f-$f1$ energy transfer rates (not shown for 260 kW and 380 kW in this Letter due to space constraints) show that the turbulent fluctuations with frequencies from 20 to 80 kHz lose energy to both ZFs and GAMs. When the ECRH power was increased from 0 to 260 kW and then to 380 kW as indicated by the black, blue, and green lines, respectively, the energy transfer to GAMs nearly tripled, but then when the heating power was increased further the energy transfer to GAMs began to decrease rapidly. However the energy transfer from turbulence to low-frequency ZFs monotonically increased as the ECRH power was increased up to 530 kW. By normalizing the energy transfer rate using the perpendicular velocity autopower, shown in Fig. 2(b), we can find the frequency-resolved effective growth rate, $\gamma_{NL}(f) = T_v(f)/\tilde{v}^2_\perp(f)$ due to energy transfer, shown in Fig. 2(d). For the turbulence frequency region that peaks at 30–40 kHz, the effective damping rate of turbulence due to the nonlinear energy transfer into ZFs and GAMs is $\gamma_{\mathrm{NL}} \approx -5 \times 10^4$ Hz, which is $\gamma_{\mathrm{NL}} \approx 0.3$–$1 \times \tilde{\omega}_{\mathrm{eddy}}$ and $\gamma_{\mathrm{NL}} \approx 0.2\omega_{\mathrm{shear}}$, indicating that the energy transfer is beginning to become comparable to other critical turbulence rates, and thus is beginning to be large enough to affect the turbulence saturation level and the turbulence dynamics. It is also clear that there is a competition between ZFs and GAMs in extracting energy from turbulence, and at the highest heating power the transfer rate into ZFs approaches that of the GAMs. If the energy transfer into the ZFs continues to grow as the heating power is increased further and begins to approach the L-H transition power threshold, which is strongly suggested by the data here, then the ZFs should play a leading role for causing the L-H confinement mode transition. Recently a novel model including the multiple shearing features with two predators (ZFs and GAMs) and one prey (turbulence) was proposed [29] which could be used to explain this competition between GAMs and ZFs for turbulent energy. The frequency resolution of the power spectra in Figs. 2(a) and 2(b) is higher than that of the energy transfer curves in Figs. 2(c) and 2(d) since bispectra converge slower than autospectra and we therefore used a narrower window for the bispectral calculation in order to have sufficient ensembles. For the discharge with 730 kW of ECRH, the probe was overheated within 20–30 ms and thus the data sequences are not long enough for the bispectra to converge; therefore the corresponding curves are not shown in Figs. 2(c) and 2(d). We also note that although most of the turbulent kinetic energy is transferred to the large-scale shear flows, the turbulent energy with intermediate frequencies is also nonlinearly transferred to fluctuations with higher frequencies (> 80 kHz), as is shown in Figs. 2(c) and 2(d). This is consistent with the observed spectral broadening of 2D turbulence [37].

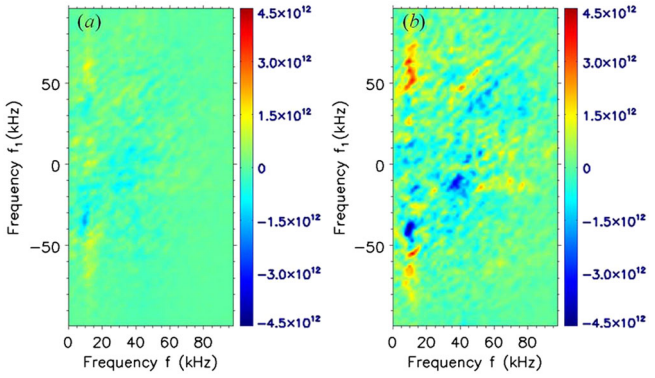

FIG. 3 (color online). Nonlinear kinetic energy transfer measured by the Langmiur probe array for (a) Ohmic plasma (b) ECRH = 530 kW. The x axis corresponds to the frequencies associated with perpendicular velocity fluctuations and the y axis corresponds to the frequencies associated with vorticity fluctuations. A positive (yellow or red) value means that the perpendicular velocity fluctuation indicated by the frequency on x axis is gaining energy and a negative value (blue) means that this velocity fluctuation frequency is losing energy.

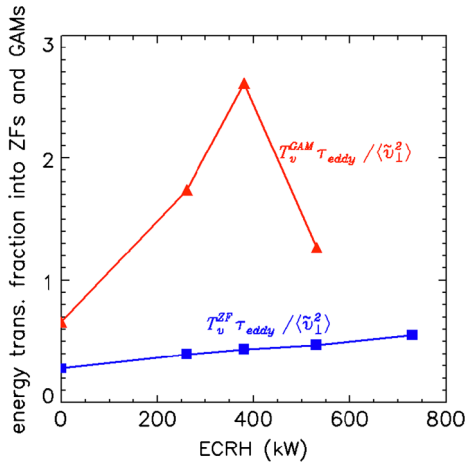

FIG. 4 (color online). Total energy transferred within a turbulence characteristic time (here 25 μs is used, corresponding to 40 kHz fluctuation) normalized by total turbulent energy, i.e., $T_v^{\mathrm{ZF}}\tau_c/\langle\tilde{v}^2_\perp\rangle$ and $T_v^{\mathrm{GAM}}\tau_c/\langle\tilde{v}^2_\perp\rangle$. Energy transfer into ZFs (blue square) and energy transfer into GAMs (red triangle).

To give an impression of how fast energy can be pumped out from turbulence due to the energy transfer, we normalized the total energy transferred into ZFs and GAMs within a turbulence characteristic time τ_c by the total turbulent fluctuation energy, i.e., $T_v^{\mathrm{ZF}}\tau_c/\langle\tilde{v}_\perp^2\rangle$ and $T_v^{\mathrm{GAM}}\tau_c/\langle\tilde{v}_\perp^2\rangle$. The results are shown in Fig. 4. Here since the turbulence spectra peak roughly at 40 kHz for all heating power [see Fig. 2(a)], we estimated $\tau_c \approx \frac{1}{40\ \mathrm{kHz}} = 25\ \mu\mathrm{s}$. T_v^{ZF} and T_v^{GAM} were estimated by integrating Fig. 2(c) over 0–5 kHz and 8–12 kHz, respectively. Values for estimating $\langle\tilde{v}_\perp^2\rangle$ were taken from Fig. 2(b), and the energy transfer for 730 kW came from Fig. 1(f). We can see in Fig. 4 that the energy transfer into ZFs monotonically increases as the heating power increases, and with 730 kW heating 50% of the turbulent energy could be transferred into ZFs within a time scale of τ_{eddy}. Note that the total energy transfer into ZFs could be greatly underestimated since $T_v(f < 1\ \mathrm{kHz})$ might be much larger than $T_v(1\ \mathrm{kHz} < f < 5\ \mathrm{kHz})$ as we can expect from Figs. 2(a) and 2(b). Compared to ZFs, the energy transfer into GAMs peaks at 380 kW and then decreases as the heating is increased. A value above 1 means that the energy associated with turbulent eddies is drained before they can complete one fluctuation cycle. Thus in weakly heated L-mode discharges, GAMs' effects on turbulence saturation would appear to dominate those of low-frequency ZFs. Then as the heating power is increased towards the L-H transition power threshold, ZFs begin to be the dominant shearing effect, and have a transfer rate that is of the same order-of-magnitude as the sheared $E \times B$ decorrelation rates and eddy decorrelation rates estimated above.

In conclusion, the energy transfer rates among turbulence, ZFs, and GAMs were unambiguously measured using two independent methods in plasmas from Ohmic to the strongly heated L-mode regimes. The results show that the turbulent kinetic energy is transferred from turbulence with intermediate frequencies (20–80 kHz) into both ZFs and GAMs, and into fluctuations with higher frequencies (> 80 kHz). The effective turbulence damping rate due to nonlinear energy transfer was inferred, and found to be $\gamma_{\mathrm{NL}} \approx 0.3\text{–}1 \times \tilde{\omega}_{\mathrm{eddy}}$ and $\gamma_{\mathrm{NL}} \approx 0.2\omega_{\mathrm{shear}}$, indicating that the energy transfer is large enough to affect the turbulence saturation level and turbulence dynamics. As the heating power increases, the energy transfer into GAMs first increases then decreases while the energy transfer into ZFs and ZFs themselves increase monotonically. This indicates a competition for turbulent energy transfer between ZFs and GAMs and suggests the leading role of ZFs in the L-H transition. Similar measurements of energy transfer rate in the recently observed turbulence-ZF limit cycle regimes [9] could thus provide definitive understanding of the role that ZFs may play in the L-H transition.

The authors would like to thank the HL-2A team for machine operation. This research is performed under the U.S. Department of Energy DOE Grant No. DE-FG02-OER54871 and is partly supported by the National Science Foundation of China Grant No. 11175060, and the National Magnetic Confinement Fusion Science Program Grant 2010GB106008.

[1] P. H. Diamond, S. I. Itoh, K. Itoh, and T. S. Hahm, Plasma Phys. Control. Fusion **47**, R35 (2005).
[2] K. Itoh and S. I. Itoh, Phys. Plasmas **13**, 055502 (2006).
[3] P. W. Terry, Rev. Mod. Phys. **72**, 109 (2000).
[4] P. H. Diamond and Y. B. Kim, Phys. Fluids B **3**, 1626 (1991).
[5] P. H. Diamond *et al.*, Nucl. Fusion **49**, 045002 (2009).
[6] G. R. Tynan, A. Fujisawa, and G. McKee, Plasma Phys. Controlled Fusion **51**, 113001 (2009).
[7] A. Fujisawa, Nucl. Fusion **49**, 013001 (2009).
[8] K. Itoh and S. I. Itoh, Plasma Phys. Control. Fusion **38**, 1 (1996).
[9] G. D. Conway *et al.*, Phys. Rev. Lett. **106**, 065001 (2011).
[10] S. J. Zweben *et al.*, Phys. Plasmas **17**, 102502 (2010).
[11] L. Schmitz *et al.*, Nucl. Fusion **49**, 095004 (2009).
[12] G. S. Xu *et al.*, Phys. Rev. Lett. **107**, 125001 (2011).
[13] C. Hidalgo, Plasma Phys. Control. Fusion **53**, 074003 (2011).
[14] T. Estrada *et al.*, Europhys. Lett. **92**, 35001 (2010).
[15] M. Xu, G. R. Tynan, C. Holland, Z. Yan, S. H. Muller, and J. H. Yu, Phys. Plasmas **16** 042312 (2009).
[16] B. Ph. van. Milligen *et al.*, Nucl. Fusion **48**, 115003 (2008).
[17] Y. Nagashima *et al.*, Plasma Phys. Control. Fusion **48**, S1 (2006).
[18] E. Sanchez *et al.*, J. Nucl. Mater. **337–339**, 296 (2005).
[19] B. Goncalves *et al.*, Phys. Rev. Lett. **96**, 145001 (2006).
[20] C. P. Ritz, E. J. Powers, and R. D. Bengtson, Phys. Fluids B **1**, 153 (1989).
[21] P. Manz, M. Ramisch, and U. Stroth, Phys. Rev. Lett. **103**, 165004 (2009).
[22] P. Manz, M. Ramisch, U. Stroth, Plasma Phys. Controlled Fusion **51**, 035008 (2009).
[23] M. Xu, G. R. Tynan, C. Holland, Z. Yan, S. H. Mueller, and J. H. Yu, Phys. Plasmas **17**, 032311 (2010).
[24] M. Xu, G. R. Tynan, P. H. Diamond, C. Holland, J. H. Yu, and Z. Yan, Phys. Rev. Lett. **107**, 055003 (2011).
[25] P. Manz *et al.*, Plasma Phys. Control. Fusion **53**, 095001 (2011).
[26] P. Manz *et al.*, Phys. Plasmas **19**, 012309 (2012).
[27] L. Chen *et al.*, Phys. Plasmas **7**, 3129 (2000).
[28] S. Benkadda *et al.*, Phys. Plasmas **18**, 052306 (2011).
[29] K. Miki and P. H. Diamond, Nucl. Fusion **51**, 103003 (2011).
[30] K. J. Zhao *et al.*, Nucl. Fusion **49**, 085027 (2009).
[31] T. Lan *et al.*, Plasma Phys. Controlled Fusion **50**, 045002 (2008).
[32] K. J. Zhao *et al.*, Phys. Rev. Lett. **96**, 255004 (2006).
[33] Nicolas Fedorczak, Ph.D. thesis, Research Institute for Magnetic Fusion, CEA Cadarache, 2010, p. 43.
[34] J. H. Yu, C. Holland, G. R. Tynan, G. Antar and Z. Yan, J. Nucl. Mater. **363–365**, 728 (2007).
[35] X. R. Duan, X. T. Ding, J. Q. Dong *et al.*, Nucl. Fusion **49**, 104012 (2009).
[36] L. W. Yan, J. Cheng, and W. Y. Hong *et al.*, Nucl. Fusion **47**, 1673 (2007).
[37] Patrick H. Diamond, Sanae-I Itoh, and Kimitaka Itoh, *Modern Plasma Physics, Volume 1: Physical Kinetics of Turbulent Plasmas* (Cambridge University Press, Cambridge, England, 2010).